First-order shear deformation analysis of rectilinear orthotropic composite circular plates undergoing transversal loads

Valerio G. Belardi[a], Pierluigi Fanelli[b], Francesco Vivio[a,*]

[a]*Department of Enterprise Engineering - University of Rome Tor Vergata, Via del Politecnico, 1, 00133, Rome, Italy*
[b]*Department of Economics, Engineering, Society and Business Organization, University of Tuscia, Largo dell'Università, 01100 Viterbo, Italy*

Abstract

This work outlines the elastic bending analysis of transversally loaded shear-deformable rectilinear orthotropic composite annular plates. The load condition discussed in the paper, along with the displacement constraints, are derived by the composite bolted joints theoretical reference model – this analytical solution is a necessary effort for the obtainment of a custom finite element capable of simulating this kind of joints with high accuracy and limited computational effort. Firstly, the constitutive equations of the family of plate under investigation are obtained in the framework of the first-order shear deformation theory. The described methodology is founded on the application of the virtual displacements principle and its solution is performed according to Ritz method after the writing of displacement field approximation functions fulfilling the boundary conditions. The three unknown displacement components are obtained for different case studies concerning rectilinear orthotropic composite annular plates featuring various slenderness ratios, shape factors and stacking sequences. The outcomes comparison with FE numerical solutions evidences a high degree of fidelity. The presented results demonstrate that this enhanced version of the Ritz analytical solution method, which accounts for the composite plate shear deformability, can be more effectively employed to describe the displacement field of composite plates connected by a bolted joint in the area surrounding the bolt.

Keywords: Rectilinear orthotropic composite material; Circular plates; First-order shear deformation plate theory; Bolted connections; Ritz method

1. Introduction

Common and advanced engineering applications in many fields such as the aerospace, aeronautical and automotive industrial sectors make a wide and constantly increasing use of composite material components because of the elevated possibilities of achieving a substantial mass budget reduction along with a remarkable structural efficiency which they guarantee in comparison with conventional metallic parts. As a consequence, other mechanical design aspects must be considered in dealing with composite shells applications, such as the need of joining together different composite parts, or composite and metal parts, and in this order of ideas bolted joints connections represent one of the widest employed joint technique. Consequently, these connections must be modeled and simulated adequately in order to perform reliable structural analyses since their failure can jeopardize the overall project integrity.

These aspects imply the necessity of adapting and transferring the knowledge and the expertise acquired in the design and simulation of traditional spot/bolted connections for metal sheets applications to the novel generation of composite components. Hence, the proper simulation, through detailed three-dimensional FE models, of these connections is highly relevant as pointed out by the broad literature referred to this subject [1–7]. Aeronautical and aerospace industries are the main fields experiencing a continuously increasing employment of composite material components to replace preexisting metallic ones with the objective of obtaining greater stiffness and strength properties per unit mass; thus, bolted joints connecting composite material or composite-metal components find extensive applications in these sectors [5, 6, 8–10]. As an example, in the design of aerospace launchers, anisogrid composite lattice structures are progressively substituting conventional metallic counterparts [11, 12] and, in this regard, the problematic of adequately simulate the bolted joints connecting the composite lattice shells endings to aluminum flanges is important.

Subsequently, the authors' purpose is the definition of a custom Spot Joint Element capable of describing the structural behavior of a region surrounding the bolted joint, comprising the bolt and a circular portion of both the plates. The Spot Joint Element definition is in accordance with a finite element assembly originally developed for the analysis of spot welded joint for metal sheets or riveted joints [13]. The great benefits belonging to this simulation tool are represented by the heavily reduced

*Corresponding author. Tel.: +39 06 72597123.
Email address: vivio@uniroma2.it (Francesco Vivio)

number of DOFs involved in the FE analysis of the spot joint without any loss in the results accuracy; therefore, this simulation technique is markedly effective in the study of multi-jointed structures [14, 15].

The stiffness matrix of the user-defined finite element is obtained through the solution of the spot joint theoretical reference model. In the original formulation of the Spot Joint Element, the theoretical formulation of this element is derived from the full analytical solution of the spot joint theoretical reference model which consists in an annular plate with isotropic material properties featuring a rigid core (when a bolt connection is considered) acting the inner edge of the plate and blocked at the outer radius. Aiming to enlarge the application field of the Spot Joint Element, this consolidated FE architecture can be further enhanced to include the FE simulation of composite bolted joints, considering a new theoretical reference model in which the annular plate is made of rectilinear orthotropic composite material. In this case, the annular plate is a laminate consisting of fiber reinforced layers in which the fibers are disposed along rectilinear directions, meanwhile the overall geometry is axisymmetric; it follows that the plate stiffness properties are are circumferentially variable.

The published literature regarding the analysis of composite circular plates is wide and varied and it covers various aspects according to different necessities. The initial efforts in this direction belong to Lekhnitskii [16, 17], who realized a preliminary analysis concerning the deflection of elliptic and circular plates.

The first study concerning elastic stability assessment of rectilinear anisotropic circular plates belongs to Tang [18]. Elastic instability of polar orthotropic annular plates is investigated in Ref. [19], the authors provide a solution in order to define buckled and post-buckled states of the composite plates. The problem of buckling resistance is deepened by Fu and Waas in Ref. [20], they describe the solution through Rayleigh-Ritz method of the problem of annular plate subject to internal or external pressure distribution. The work accounts for both rectilinear and polar orthotropic material properties. Moreover, Seifi et al. [21] studied the elastic instability problem cross-ply laminated annular plates, under the thin-plates assumption according to symmetric buckling loads.

With reference to the modal behavior of rectilinear orthotropic composite circular plates, Rajappa [22] determined natural frequencies and mode shapes of clamped circular plates making use of Galerkin method. Analogously, in Ref. [23] the same characteristics are determined through the employment of the least-squares interior collocation method. Furthermore, Nallim and Grossi [24] realized the the dynamic analysis of symmetrically laminated composite and circular plates accounting for the influence of fiber orientation on the natural frequencies, the approach is based on the Rayleigh-Ritz method. Then, the Ritz solution to the 3D free vibration analysis of thick annular functionally graded plates with piezoelectric layers is outlined in Ref. [25].

A study about elastic linear and non-linear analysis of symmetrically laminated sector plates having rectilinear orthotropic characteristics was conducted in Ref. [26] by Salehi and Sobhani. The governing differential equations were derived in both linear and non-linear forms in the frame of Mindlin plate theory; then, the dynamic relaxation method in conjunction with the finite difference discretization technique were employed to discretize the equations in order to solve the problem. Laminated sector plates are further discussed in terms of non-linear static analysis in Refs. [27] accounting for first-order shear deformation theory, large deformation and Von Kármán non-linearity by means of generalized differential quadrature method. Additionally, Kadkhodayan et al. [28] investigated the elastic behavior of rectilinear orthotropic plates, featuring different shapes, assuming large deflections. The governing equations, expressed in Cartesian coordinates, are firstly discretized making use of the finite-difference method and then resolved through the application of DXDR dynamic relaxation method.

In Refs. [29, 30] the authors provided an analysis of stiffened annular functionally graded sector plates undergoing thermal and mechanical loads; material properties vary along the plate thickness direction and Von Kármán large deflection hypothesis is assumed along with first-order shear deformation plate theory obtaining nonlinear equilibrium equations which are solved exploiting the finite difference method and the dynamic relaxation method. The thermo-elastic behavior of functionally graded circular plates is also discussed [31]. Full Analytical solutions are provided for axisymmetric mechanical and thermal loads acting on the upper and lower surfaces of the plate.

Laminated sector plates featuring both polar and rectilinear orthotropic material properties are analyzed in Ref. [32], accounting for angular variability of stiffness properties in the latter case.

The bending problem of composite circular plates featuring a square hole is treated in Ref. [33]. The bending moment distribution around square hole is obtained with a known mapping function in symmetric laminates undergoing different loading conditions.

The studies of the same authors depicted in Refs. [34–37] are aimed to establish the theoretical framework of the novel Spot Joint Element; meanwhile, on the one hand, the isotropic theoretical reference model can be solved fully analytically, closed form solutions cannot be obtained after the introduction of rectilinear orthotropic material and, consequently, the elastic analyses previously conducted necessitated of approximated solutions through the employment of semi-analytical approaches based on weight residual methods or the energy approach. In particular, [35] presents an original approach which combines the bending plate theory for composite materials, in order to analytically define the governing equation of rectilinear orthotropic composite circular plates subject to transversal loads, with the use of Galerkin solution method. In addition, in Ref. [34], the same authors discussed the possibility of introducing the hypothesis of axisymmetry for the mid-surface deflection for the specific case of quasi-isotropic laminates. Moreover, after the derivation of the constitutive equations, the energy approach was considered adopting Ritz method along with the principle of virtual displacements allowing to enlarge the amount of resolvable load conditions, including both transversal and in-plane load conditions [36] and in-plane bending moment and torque moment [37]. The expressions of the approximation functions are derived according to constraints conditions and depicted in a general formulation for all load conditions.

The solution of the in-plane load condition was implemented in [38], as a first trial, in the FE stiffness matrix of the enhanced Spot Joint Element. The outcomes of FE analyses in which the novel composite bolted joint element is utilized reliably match those obtained by virtue of conventional FE models, but requiring an high number of nodes and elements.

The previous studies allow to completely determine the terms of the new Spot Joint Element stiffness matrix. However, these solutions are obtained in the frame of classical lamination plate theory (CPT) and consequently the displacement field they provide is in accordance with the kinematics hypotheses of Classical plate theory which does not account for the effect of transverse shear deformations. This implies that the solution for the transversal load condition precisely describe the actual displacement field for low slenderness ratios between thickness and outer radius, whereas the mid-surface deflection turns out be underestimated as long as this parameter is increased. Anyway, slenderness ratios usually employed in constructive practice can be affected by not negligible transverse shear deformations: this requires an improvement of the theoretical framework.

Therefore, this work aims to the definition of an original solution procedure for the transversal load condition based on the first-order shear deformation theory (FSDT) in order to precisely reproduce the displacement field of the mid-surface of the annular rectilinear orthotropic circular plates, improving previous studies realized about this topic [34–36]. Thus, the derivation of constitutive equations is outlined taking into account the plate shear deformability to set up a theoretical approach based on the application of Ritz method to solve the principle of virtual works. The general expression of the principle of virtual work is presented for the transversal load condition; additionally, specific forms of the approximation functions are derived for the mid-surface deflection and the rotations around the circumferential and the radial directions.

Then, results are presented for two symmetrical lay-ups largely employed for industrial applications and in literature regarding composite bolted joints, i.e. the quasi-isotropic (QI) and the zero-dominated (0D) ones (see Refs. [1–5, 7]). Outcomes of Ritz method showing the dependence of displacement components on both radial and circumferential coordinates are reported and compared with those of FE analyses obtained through a refined reference model. Afterward, the effect of the aspect ratio of the composite circular plate on the results is further investigated in conjunction with the slenderness ratios one.

The proposed analytical method results show a very good agreement with the outcomes of reference FE analyses, demonstrating the high reliability and accuracy of the presented method. In the end, the FSDT turns out to be more accurate of the CPT to deal with the design and the analysis of composite bolted joints.

2. First-order shear deformation plate theory constitutive equations of rectilinear orthotropic composite circular plates

A circular plate cut out from a rectangular laminate features, despite the axysimmetric geometry, a unique set of material properties principal directions and, as a consequence, its elastic behavior turns out to be dependent on the angular coordinate θ. This characteristic arises because of the particular fibers arrangement present within the layers that make up the laminate. In fact, the fibers of every layer are disposed longwise straight trajectories and form a specific angle with respect to the x-axis of the Cartesian coordinate system, Fig. 1, according to the plate stacking sequence. Because of the circumferentially variable bending stiffnesses, the bending analysis of this class of circular plates involves the solution of a bidimensional problem in order to determine the displacement field produced by the action of transversal or bending loads.

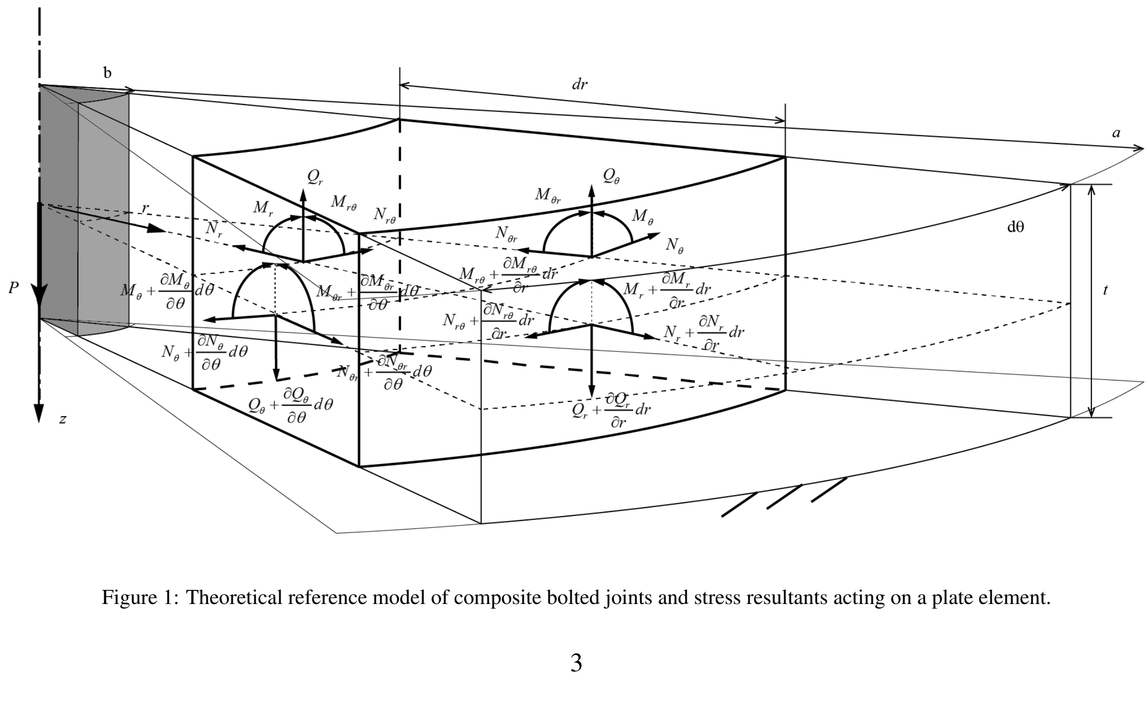

Figure 1: Theoretical reference model of composite bolted joints and stress resultants acting on a plate element.

2.1. Stress-strain relation

Nevertheless, the cylindrical coordinate system (r, θ, z) is more suitable in order to perform the investigation of rectilinear orthotropic composite circular plates. Therefore, the starting point of the analysis is represented by the definition of the stress-strain relation for a generic k^{th} rectilinear orthotropic layer building up a laminate circular plate in cylindrical coordinates; these expression can be obtained by means of the application of the rotation matrix $\left[T(\theta)\right]$ to the stress and strains vectors expressed in Cartesian coordinates (x, y, z) as widely described in [36]:

$$\begin{Bmatrix} \sigma_r \\ \sigma_\theta \\ \tau_{\theta z} \\ \tau_{rz} \\ \tau_{r\theta} \end{Bmatrix}_k = \left[\overline{Q}(\theta)\right]_k \begin{Bmatrix} \varepsilon_r \\ \varepsilon_\theta \\ \gamma_{\theta z} \\ \gamma_{rz} \\ \gamma_{r\theta} \end{Bmatrix}_k \tag{1}$$

where the transformed reduced stiffness matrix in cylindrical coordinates $\left[\overline{Q}(\theta)\right]_k$ is obtained by means of the matrix product:

$$\begin{aligned} \left[\overline{Q}(\theta)\right]_k &= \left[T(\theta)\right]\left[\overline{Q}\right]_k\left[T(\theta)\right]^T = \\ &= \begin{bmatrix} c^2 & s^2 & 0 & 0 & 2cs \\ s^2 & c^2 & 0 & 0 & -2cs \\ 0 & 0 & c & -s & 0 \\ 0 & 0 & s & c & 0 \\ -cs & cs & 0 & 0 & c^2-s^2 \end{bmatrix} \begin{bmatrix} \overline{Q}_{11} & \overline{Q}_{12} & 0 & 0 & \overline{Q}_{16} \\ \overline{Q}_{12} & \overline{Q}_{22} & 0 & 0 & \overline{Q}_{26} \\ 0 & 0 & \overline{Q}_{44} & \overline{Q}_{45} & 0 \\ 0 & 0 & \overline{Q}_{45} & \overline{Q}_{55} & 0 \\ \overline{Q}_{16} & \overline{Q}_{26} & 0 & 0 & \overline{Q}_{66} \end{bmatrix}_k \begin{bmatrix} c^2 & s^2 & 0 & 0 & 2cs \\ s^2 & c^2 & 0 & 0 & -2cs \\ 0 & 0 & c & -s & 0 \\ 0 & 0 & s & c & 0 \\ -cs & cs & 0 & 0 & c^2-s^2 \end{bmatrix}^T \end{aligned} \tag{2}$$

being: $c = \cos(\theta)$, $s = \sin(\theta)$ and θ the angle evaluated from the x-axis of the Cartesian coordinate system to the r-axis of the cylindrical coordinate system, Fig. 1, and $\left[\overline{Q}\right]_k$ indicates the transformed reduced stiffness matrix of the k^{th} layer expressed in the global Cartesian coordinate system.

The terms composing the reduced stiffness matrix in the cylindrical coordinate system $\left[\overline{Q}(\theta)\right]_k$ of the k^{th} rectilinear orthotropic layer are no more constants as the layer exhibits a different elastic response depending on the angular coordinate θ.

Moreover, a condition of perfect adhesion between the layers comprising the rectilinear orthotropic composite circular plate can be supposed, owing to one of the fundamental assumption encompassed in the classical lamination theory [39]. This aspect entails the displacements and strains are continuous functions alongside the plate thickness direction z and, subsequently, the comprehensive stresses of the rectilinear orthotropic composite circular plate can be derived adding up the homologous stress terms of the N layers over the thickness:

$$\begin{Bmatrix} \sigma_r \\ \sigma_\theta \\ \tau_{\theta z} \\ \tau_{rz} \\ \tau_{r\theta} \end{Bmatrix} = \sum_{k=1}^{N} \begin{Bmatrix} \sigma_r \\ \sigma_\theta \\ \tau_{\theta z} \\ \tau_{rz} \\ \tau_{r\theta} \end{Bmatrix}_k = \sum_{k=1}^{N} \left[\overline{Q}(\theta)\right]_k \begin{Bmatrix} \varepsilon_r \\ \varepsilon_\theta \\ \gamma_{\theta z} \\ \gamma_{rz} \\ \gamma_{r\theta} \end{Bmatrix} = \left[\overline{Q}(\theta)\right] \begin{Bmatrix} \varepsilon_r \\ \varepsilon_\theta \\ \gamma_{\theta z} \\ \gamma_{rz} \\ \gamma_{r\theta} \end{Bmatrix} \tag{3}$$

in which a generic term of the laminate reduced stiffness matrix in the cylindrical coordinate system is: $\overline{Q}_{ij}(\theta) = \sum_{k=1}^{N} \overline{Q}_{ij}^{(k)}(\theta)$.

2.2. Compatibility equations

As regards the kinematic assumptions, the FSDT relieves one of the basic hypotheses proper of the CPT; indeed, the normals to the plate mid-surface are no more presumed to remain perpendicular to the mid-surface when the laminate undergoes a deformation. This behavior is attained adding a constant state of transverse shear strains alongside the laminate thickness to the strain field. However, the assumptions of plane-stress state and inextensible normals are preserved; as a consequence, the mid-surface deflection w is constant in reference to the thickness coordinate z [40, 41].

Therefore, the FSDT state the components of the displacement field along the coordinate directions r, θ and z are:

$$\begin{aligned} u_r(r, \theta, z) &= u(r, \theta) + z\, \phi_r(r, \theta) \\ u_\theta(r, \theta, z) &= v(r, \theta) + z\, \phi_\theta(r, \theta) \\ u_z(r, \theta, z) &= w(r, \theta) \end{aligned} \tag{4}$$

where u, v and w denote the plate mid-surface ($z = 0$) radial, circumferential and deflection displacements respectively; whereas ϕ_r and ϕ_θ indicate the rotations of the normal to the plate mid-surface about the circumferential and radial directions.

Additionally, the strains expressed in cylindrical coordinates and related to the displacement components in (4) are:

$$
\begin{Bmatrix} \varepsilon_r \\ \varepsilon_\theta \\ \gamma_{\theta z} \\ \gamma_{rz} \\ \gamma_{r\theta} \end{Bmatrix} = \begin{Bmatrix} \dfrac{\partial u_r}{\partial r} \\ \dfrac{u_r}{r} + \dfrac{1}{r}\dfrac{\partial u_\theta}{\partial \theta} \\ \dfrac{\partial u_\theta}{\partial z} + \dfrac{1}{r}\dfrac{\partial u_z}{\partial \theta} \\ \dfrac{\partial u_r}{\partial z} + \dfrac{\partial u_z}{\partial r} \\ \dfrac{1}{r}\dfrac{\partial u_r}{\partial \theta} + \dfrac{\partial u_\theta}{\partial r} - \dfrac{u_\theta}{r} \end{Bmatrix} = \begin{Bmatrix} \varepsilon_r^0 \\ \varepsilon_\theta^0 \\ \gamma_{\theta z}^0 \\ \gamma_{rz}^0 \\ \gamma_{r\theta}^0 \end{Bmatrix} + z \begin{Bmatrix} \kappa_r \\ \kappa_\theta \\ 0 \\ 0 \\ \kappa_{r\theta} \end{Bmatrix} \tag{5}
$$

being each strain composed of two contributions, the first one represents the mid-surface strains and the latter connected to mid-surface curvatures.

Then, each strain and curvature term in (5) can be written as a function of the mid-surface displacements:

$$
\begin{aligned}
\varepsilon_r^0 &= \frac{\partial u}{\partial r} & \kappa_r &= \frac{\partial \phi_r}{\partial r} \\
\varepsilon_\theta^0 &= \frac{u}{r} + \frac{1}{r}\frac{\partial v}{\partial \theta} & \kappa_\theta &= \frac{\phi_r}{r} + \frac{1}{r}\frac{\partial \phi_\theta}{\partial \theta} \\
\gamma_{\theta z}^0 &= \phi_\theta + \frac{1}{r}\frac{\partial w}{\partial \theta} & & \\
\gamma_{rz}^0 &= \phi_r + \frac{\partial w}{\partial r} & & \\
\gamma_{r\theta}^0 &= \frac{1}{r}\frac{\partial u}{\partial \theta} + \frac{\partial v}{\partial r} - \frac{v}{r} & \kappa_{r\theta} &= \frac{1}{r}\frac{\partial \phi_r}{\partial \theta} + \frac{\partial \phi_\theta}{\partial r} - \frac{\phi_\theta}{r}
\end{aligned} \tag{6}
$$

In the end, the strain field features in-plane components of strain which linearly depend on the coordinate z and overall amounts of the transverse shear strains that do not vary alongside the composite annular plate thickness.

2.3. Stress resultants

Furthermore, the integration of the elemental forces and moments over the N-layers in the laminate thickness t returns the stress resultants per unit width:

- In-plane forces

$$
\begin{Bmatrix} N_r \\ N_\theta \\ N_{r\theta} \end{Bmatrix} = \int_{-t/2}^{t/2} \begin{Bmatrix} \sigma_r \\ \sigma_\theta \\ \tau_{r\theta} \end{Bmatrix} dz = \begin{bmatrix} A(\theta) & A_{12}(\theta) & A_{16}(\theta) \\ A_{12}(\theta) & A_{22}(\theta) & A_{26}(\theta) \\ A_{16}(\theta) & A_{26}(\theta) & A_{66}(\theta) \end{bmatrix} \begin{Bmatrix} \varepsilon_r^0 \\ \varepsilon_\theta^0 \\ \gamma_{r\theta}^0 \end{Bmatrix} + \begin{bmatrix} B_{11}(\theta) & B_{12}(\theta) & B_{16}(\theta) \\ B_{12}(\theta) & B_{22}(\theta) & B_{26}(\theta) \\ B_{16}(\theta) & B_{26}(\theta) & B_{66}(\theta) \end{bmatrix} \begin{Bmatrix} \kappa_r \\ \kappa_\theta \\ \kappa_{r\theta} \end{Bmatrix} \tag{7}
$$

- Shear forces

$$
\begin{Bmatrix} Q_\theta \\ Q_r \end{Bmatrix} = K_s \int_{-t/2}^{t/2} \begin{Bmatrix} \tau_{\theta z} \\ \tau_{rz} \end{Bmatrix} dz = K_s \begin{bmatrix} A_{44}(\theta) & A_{45}(\theta) \\ A_{45}(\theta) & A_{55}(\theta) \end{bmatrix} \begin{Bmatrix} \gamma_{\theta z}^0 \\ \gamma_{rz}^0 \end{Bmatrix} \tag{8}
$$

- Bending and torque moments

$$
\begin{Bmatrix} M_r \\ M_\theta \\ M_{r\theta} \end{Bmatrix} = \int_{-t/2}^{t/2} \begin{Bmatrix} \sigma_r \\ \sigma_\theta \\ \tau_{r\theta} \end{Bmatrix} z dz = \begin{bmatrix} B_{11}(\theta) & B_{12}(\theta) & B_{16}(\theta) \\ B_{12}(\theta) & B_{22}(\theta) & B_{26}(\theta) \\ B_{16}(\theta) & B_{26}(\theta) & B_{66}(\theta) \end{bmatrix} \begin{Bmatrix} \varepsilon_r^0 \\ \varepsilon_\theta^0 \\ \gamma_{r\theta}^0 \end{Bmatrix} + \begin{bmatrix} D_{11}(\theta) & D_{12}(\theta) & D_{16}(\theta) \\ D_{12}(\theta) & D_{22}(\theta) & D_{26}(\theta) \\ D_{16}(\theta) & D_{26}(\theta) & D_{66}(\theta) \end{bmatrix} \begin{Bmatrix} \kappa_r \\ \kappa_\theta \\ \kappa_{r\theta} \end{Bmatrix} \tag{9}
$$

The coefficient $K_s = \frac{5}{6}$ present in Eq. (8) is the shear correction factor needed to adjust the approximation introduced by the FSDT kinematic hypotheses which introduces a constant, over the thickness, distribution of shear stress which instead is of higher order.

Regarding the stiffness matrices proper of the expressions of stress resultants (7-9), the stiffness coefficients dependent on the angular coordinate θ are defined as:

$$
\begin{aligned}
\Big(A_{ij}(\theta),\ B_{ij}(\theta),\ D_{ij}(\theta)\Big) &= \int_{-t/2}^{t/2} \overline{Q}_{ij}^{(k)}(\theta)\Big(1,\ z,\ z^2\Big)dz \\
&= \Big(1,\ \frac{1}{2},\ \frac{1}{3}\Big) \sum_{k=1}^{N} \overline{Q}_{ij}^{(k)}(\theta)\Big((z_k,\ z_k^2,\ z_k^3) - (z_{k-1},\ z_{k-1}^2,\ z_{k-1}^3)\Big)
\end{aligned} \tag{10}
$$

where: $A_{ij}(\theta)$ are the extensional stiffnesses, $B_{ij}(\theta)$ the bending-extension coupling stiffnesses and $D_{ij}(\theta)$ the bending stiffnesses for a rectilinear orthotropic composite circular plate expressed in the cylindrical coordinate system. In addition, z_k and z_{k-1} are the oriented distances to the bottom and the top, respectively, of the k^{th} layer.

3. Application of Ritz method to principle of virtual displacements

The presented procedure is based on Ritz method which must be employed in conjunction with the principle of virtual displacements, as outlined in [36], in order to take into account the natural boundary conditions of the specific problem. The principle of virtual displacements for a rectilinear orthotropic circular plate undergoing transversal loads states:

$$\begin{aligned}\delta W = \delta W_I + \delta W_E = 0 = &\int_{\Omega} \Big(\sigma_r\, \delta\varepsilon_r + \sigma_\theta\, \delta\varepsilon_\theta + \tau_{\theta z}\, \delta\gamma_{\theta z} + \tau_{rz}\, \delta\gamma_{rz} + \tau_{r\theta}\, \delta\gamma_{r\theta}\Big)\, d\Omega \\ &- \int_{-\pi}^{\pi} \Big(b\, Q_b\, \delta w(b,\theta) - a\, Q_a\, \delta w(a,\theta)\Big)\, d\theta\, - \int_b^a \int_{-\pi}^{\pi} q(r,\theta)\, \delta w(r,\theta)\, d\theta\, rdr\end{aligned} \tag{11}$$

in which: δW_I and δW_E are the internal and the external virtual works. Additionally, the symbol δ is utilized to denote virtual displacements and strains, Ω is the circular plate analytical integration region, meanwhile $d\Omega$ is the infinitesimal volume element. As regards the external loads involved in the transversal load condition, they act along directions perpendicular to the plate mid-surface, they are: distributed forces per unit-length acting at the outer or at the inner plate edge, Q_a and Q_b respectively, or a distributed load $q(r,\theta)$.

With reference to the solution method provided in [36] in the framework of CPT for the transversal load condition, the internal virtual work δW_I assumes a different formulation since the analysis is realized according to an enhanced theoretical background; meanwhile the external virtual work δW_E is formally unvaried. Additionally, it should be noted that the employment of the FSDT implies the determination of three independent displacement components: the mid-surface deflection $w(r,\theta)$ and the rotations of the normal to the plate mid-surface about the circumferential and radial directions, $\phi_r(r,\theta)$ and $\phi_\theta(r,\theta)$ respectively; whereas the previously described analysis founded on the CPT exclusively required the solution of the plate mid-surface deflection as the two rotation components were dependent on the deflection.

Then, specifically, as regards the transversal load condition of the theoretical reference model (Fig. 1), i.e. a composite annular plate characterized by rectilinear orthotropic material properties with clamped constraint conditions at the outer edge and presenting a rigid core at the inner one undergoing external loads orthogonal to its mid-surface, the generic formulation of the internal virtual work is:

$$\begin{aligned}\delta W_I = \int_b^a \int_{-\pi}^{\pi} \Big[&N_r \frac{\partial \delta u}{\partial r} + N_\theta\Big(\frac{\delta u}{r} + \frac{1}{r}\frac{\partial \delta v}{\partial \theta}\Big) + N_{r\theta}\Big(\frac{1}{r}\frac{\partial \delta u}{\partial \theta} + \frac{\partial \delta v}{\partial r}\Big) + Q_\theta\Big(\delta\phi_\theta + \frac{1}{r}\frac{\partial \delta w}{\partial \theta}\Big) + Q_r\Big(\delta\phi_r + \frac{\partial \delta w}{\partial r}\Big) + \\ &+ M_r \frac{\partial \delta\phi_r}{\partial r} + M_\theta\Big(\frac{\delta\phi_r}{r} + \frac{1}{r}\frac{\partial \delta\phi_\theta}{\partial \theta}\Big) + M_{r\theta}\Big(\frac{1}{r}\frac{\partial \delta\phi_r}{\partial \theta} + \frac{\partial \delta\phi_\theta}{\partial r} - \frac{\delta\phi_\theta}{r}\Big)\Big]\, d\theta\, rdr\end{aligned} \tag{12}$$

As a consequence of the action of external loads perpendicularly to the composite annular plate mid-surface, both the in-plane displacement components, i.e. the radial u and the circumferential v, vanish; meanwhile the three unknown displacement components are other than zero and must be obtained according to the solution method. Moreover, it should be considered that the bending-extension coupling stiffness terms $B_{ij}(\theta)$ are all null as a result of the lay-up symmetry in reference to the composite plate mid-surface. In addition, no membrane-shell coupling effect is activated by the transversal loads because of the linear strain-displacement relations were taken into account. Thus, it can be concluded that the in-plane stress resultants vanish, whereas the bending and the torque moments in (9) are exclusively function of the curvatures.

Besides, accounting for the transversal load condition, the theoretical reference model of composite bolted joint introduces the following boundary conditions:

- Outer edge of the plate: $r = a$

$$\begin{aligned}&(I)\ w(a,\theta) = 0 \\ &(II)\ \phi_r(a,\theta) = 0 \\ &(III)\ \phi_\theta(a,\theta) = 0\end{aligned} \tag{13}$$

- Inner edge of the plate: $r = b$

$$
\begin{aligned}
&(IV)\ w(b,\theta) = const\ \ \forall\theta \Rightarrow \ \frac{\partial w(b,\theta)}{\partial\theta} = 0 \\
&(V)\ \phi_r(b,\theta) = 0 \\
&(VI)\ \phi_\theta(b,\theta) = 0
\end{aligned}
\tag{14}
$$

The boundary conditions prescribed at the outer edge of the annular plate, because of the clamping constraint conditions, require that the deflection and the rotations around both the circumferential and the radial directions must be all null, as stated by conditions (I), (II) and (III) respectively. On the other hand, the boundary conditions defined at the inner edge and deriving from the rigid core address: uniform deflection at the inner edge, i.e. invariant with the circumferential coordinate θ, as outlined by condition (IV); then, null rotations about the circumferential and the radial directions at the inner radius are demanded by conditions (V) and (VI).

Furthermore, the Ritz method statements impose the components of the displacement field to be formulated through the summation of a complete set of continuous and linearly independent approximation functions, each one weighted by means of unknown scalar coefficients. In addition, it must be considered that in consequence of the dependence of the bending stiffnesses on the circumferential coordinate, the three unknown displacement components of the rectilinear orthotropic composite circular are not axisymmetric, being function of the angular coordinate θ in accordance with a trigonometric function. Therefore, the approximate form of the mid-plate transversal displacement and the rotations about the circumferential and radial directions, i.e. $W_N(r,\theta)$, $\Phi_r^N(r,\theta)$ and $\Phi_\theta^N(r,\theta)$ respectively, are defined by means of the summation of two contributions: firstly, the medium contribution of the displacement field component which is independent from the angular coordinate θ; the second one represents the angular perturbation provoked by the not-axisymmetry of the material properties on the medium component of displacement. Thus, the approximate form of the three displacement components to be determined are expressed as the summation of two contributions:

- Approximate mid-surface deflection

$$
w(r,\theta) \approx W_N(r,\theta) = \overline{W}_M(r) + \widetilde{W}_N(r,\theta) = \sum_{j=1}^{M_\alpha} c_j\ \varphi_j(r)\ +\sum_{j=M_\alpha+1}^{N_\alpha} c_j\ \varphi_j(r,\theta) \tag{15}
$$

- Approximate rotation about the circumferential direction

$$
\phi_r(r,\theta) \approx \Phi_r^N(r,\theta) = \bar{\Phi}_r^M(r) + \widetilde{\Phi}_r^N(r,\theta) = \sum_{l=1}^{M_\beta} k_l\ \psi_l(r)\ +\sum_{l=M_\beta+1}^{N_\beta} k_l\ \psi_l(r,\theta) \tag{16}
$$

- Approximate rotation about the radial direction

$$
\phi_\theta(r,\theta) \approx \Phi_\theta^N(r,\theta) = \bar{\Phi}_\theta^M(r) + \widetilde{\Phi}_\theta^N(r,\theta) = \sum_{n=1}^{M_\gamma} h_n\ \lambda_n(r)\ +\sum_{n=M_\gamma+1}^{N_\gamma} h_n\ \lambda_n(r,\theta) \tag{17}
$$

where c_j, k_l and h_n are the unknown scalar coefficients of the three approximate displacement components to be determined. In Eqs. (15-17), the first series $\overline{W}_M(r)$, $\bar{\Phi}_r^M(r)$ and $\bar{\Phi}_\theta^M(r)$ represent the medium and axisymmetric contribution of displacement component, the second ones $\widetilde{W}_N(r,\theta)$, $\widetilde{\Phi}_r^N(r,\theta)$ and $\widetilde{\Phi}_\theta^N(r,\theta)$ are the contributions for the angular perturbation needed to take into account the variable bending stiffnesses. Further, the subscripts α, β and γ are employed because, in general, the number of terms in the series of the approximate displacement components are different.

The approximation functions $\varphi_j(r,\theta)$, $\psi_l(r,\theta)$ and $\lambda_n(r,\theta)$ for the angular perturbation contribution of the mid-surface deflection w and the rotations about the circumferential and the radial directions, ϕ_r and ϕ_θ, are obtained through the product of two functions: the first one is function of the only radial coordinate r, and the second one function that is, contrariwise, exclusively dependent on the angular coordinate θ:

$$
\begin{aligned}
\varphi_j(r,\theta) &= p_j(r)\ g(\theta) \\
\psi_l(r,\theta) &= p_l(r)\ g(\theta) \\
\lambda_n(r,\theta) &= p_n(r)\ \frac{dg(\theta)}{d\theta}
\end{aligned}
\tag{18}
$$

in which the functions $p(r)$ are employed for the radial dependent contribution of all three displacement components because they have to satisfy the same boundary conditions.

Moreover, it can be concluded that the functions $p(r)$ can be utilized even to describe the axisymmetric contribution of the rotations ϕ_r and ϕ_θ, i.e.:

$$\begin{aligned}\psi_l(r) &= p_l(r)\\ \lambda_n(r) &= p_n(r)\end{aligned} \tag{19}$$

Moreover, according to the transversal displacement of the annular plate mid-surface, the functions $p(r)$ are needed to respect the boundary conditions (13) and (14). Thus, so as to fulfill the boundary condition (IV) requiring a uniform mid-surface deflection at the annular plate inner edge, the series $\widetilde{W}_N(r,\theta)$ must be null if evaluated at the inner radius b, despite the effective deflection at that radial coordinate does not vanish. Hence, this aspect contributes to clarify the role played by the summation $\widetilde{W}_N(r,\theta)$: it is accountable for the variation with the angular coordinate θ of the composite annular plate transversal displacement caused by the circumferentially variable bending stiffnesses.

With reference to the trigonometric function $g(\theta)$, this function of the angular coordinate θ is necessary to account for the circumferential fluctuation of the displacement field components and it must be particularized depending on the lay-up featured by the annular plate. As regards the symmetrical lay-ups utilized for the numerical examples outlined in the following Section, two trigonometric functions $g(\theta)$ are employed:

- QI lay-up

$$g(\theta) = \sin\left(2\theta + \frac{\pi}{4}\right) \tag{20}$$

- 0D lay-up

$$g(\theta) = \cos\left(2\theta - \frac{\pi}{8}\right) \tag{21}$$

Additionally, the case studies hereafter discussed in Section 4 make use of series $W_N(r,\theta)$, $\Phi_r^N(r,\theta)$ and $\Phi_\theta^N(r,\theta)$ composed of 10 terms; in particular, 5 terms series to represent the medium and axisymmetric contribution of displacement component and 5 for the not-axisymmetric ones. Both the approximation functions $\varphi_j(r)$ and the functions $p(r)$ employed in the numerical examples are of polynomial type and cannot be expressed through a general form, so the they are listed in the Appendix Sections.

Once the approximation functions have been selected, Ritz method addresses the substitution of the approximate form of the displacement components (15-17) in the energy principle, i.e. the virtual displacement statement outlined in (11) in this case. By virtue of this substitution, the principle of virtual displacements depends only on the N unknown coefficients. Then, its validity must be assured for every admissible virtual displacement obtained with the δc_i coefficients, this requirement implies the validity of the principle of virtual displacements independently from these coefficients:

$$\delta W(S_N) = \sum_{i=1}^{N} \frac{\partial W}{\partial c_i}\delta c_i = 0 \quad \forall \delta c_i \quad \Rightarrow \quad \frac{\partial W}{\partial c_i} = 0 \tag{22}$$

The validity of Eq. (22) requires the solution of a linear system of N algebraic equations to find the N unknown coefficients; each equation is of the type:

$$\sum_{j=1}^{N} R_{ij}\, c_j - F_i = 0, \qquad i = 1, 2, \ldots, N \tag{23}$$

in which the coefficient matrix terms R_{ij} are depend on the approximation functions, material properties and plate geometry, whereas the known terms F_i are function of the external loads.

For what concerns the determination of the unknown scalar coefficients c_j, k_l and h_n, the substitution of the approximate form of the displacement components outlined in Eqs. (15-17) in the principle of virtual displacements (22) returns a linear system of the type (23):

$$\left[\begin{array}{c|c|c} R_{ij}^{N_\alpha x N_\alpha} & R_{il}^{N_\alpha x N_\beta} & R_{in}^{N_\alpha x N_\gamma} \\ \hline R_{kj}^{N_\beta x N_\alpha} & R_{kl}^{N_\beta x N_\beta} & R_{kn}^{N_\beta x N_\gamma} \\ \hline R_{mj}^{N_\gamma x N_\alpha} & R_{ml}^{N_\gamma x N_\beta} & R_{mn}^{N_\gamma x N_\gamma} \end{array}\right] \begin{Bmatrix} \vdots \\ c_j \\ \vdots \\ k_l \\ \vdots \\ h_n \\ \vdots \end{Bmatrix} = \begin{Bmatrix} \vdots \\ F_i \\ \vdots \\ 0 \\ \vdots \\ 0 \\ \vdots \end{Bmatrix} \tag{24}$$

The coefficient matrix of the system of algebraic equations (24) is made up of various submatrices whose elements are:

$$
\begin{aligned}
R_{ij} &= \int_b^a \int_{-\pi}^{\pi} \left\{\Phi_i\right\}^T \left[A(\theta)\right] \left\{\Phi_j\right\} \, d\theta \, rdr \\
R_{il} &= \int_b^a \int_{-\pi}^{\pi} \left\{\Phi_i\right\}^T \left[A_1(\theta)\right] \psi_l \, d\theta \, rdr \\
R_{in} &= \int_b^a \int_{-\pi}^{\pi} \left\{\Phi_i\right\}^T \left[A_2(\theta)\right] \lambda_n \, d\theta \, rdr \\
R_{kj} &= \int_b^a \int_{-\pi}^{\pi} \psi_k \left[A_1(\theta)\right]^T \left\{\Phi_j\right\} \, d\theta \, rdr \\
R_{kl} &= \int_b^a \int_{-\pi}^{\pi} \left(\left\{\Psi_k\right\}^T \left[D(\theta)\right] \left\{\Psi_l\right\} + A_{55}(\theta)\psi_k\psi_l \right) d\theta \, rdr \\
R_{kn} &= \int_b^a \int_{-\pi}^{\pi} \left(\left\{\Psi_k\right\}^T \left[D_1(\theta)\right] \left\{\Lambda_n\right\} + A_{45}(\theta)\psi_k\lambda_n \right) d\theta \, rdr \\
R_{mj} &= \int_b^a \int_{-\pi}^{\pi} \lambda_m \left[A_2(\theta)\right]^T \left\{\Phi_j\right\} \, d\theta \, rdr \\
R_{ml} &= \int_b^a \int_{-\pi}^{\pi} \left(\left\{\Lambda_m\right\}^T \left[D_1(\theta)\right]^T \left\{\Psi_l\right\} + A_{45}(\theta)\lambda_m\psi_l \right) d\theta \, rdr \\
R_{mn} &= \int_b^a \int_{-\pi}^{\pi} \left(\left\{\Lambda_m\right\}^T \left[D_2(\theta)\right] \left\{\Lambda_n\right\} + A_{44}(\theta)\lambda_m\lambda_n \right) d\theta \, rdr
\end{aligned}
\tag{25}
$$

where:

$$
\left\{\Phi_{i,j}\right\} = \begin{Bmatrix} \frac{1}{r}\frac{\partial \varphi_{i,j}}{\partial \theta} \\ \frac{\partial \varphi_{i,j}}{\partial r} \end{Bmatrix} \qquad \left\{\Psi_{k,l}\right\} = \begin{Bmatrix} \frac{\partial \psi_{k,l}}{\partial r} \\ \frac{\psi_{k,l}}{r} \\ \frac{1}{r}\frac{\partial \psi_{k,l}}{\partial \theta} \end{Bmatrix} \qquad \left\{\Lambda_{m,n}\right\} = \begin{Bmatrix} \frac{1}{r}\frac{\partial \lambda_{m,n}}{\partial \theta} \\ \frac{\partial \lambda_{m,n}}{\partial r} - \frac{\lambda_{m,n}}{r} \end{Bmatrix} \tag{26}
$$

$$
\left[A_1(\theta)\right] = \begin{bmatrix} A_{45}(\theta) \\ A_{55}(\theta) \end{bmatrix} \qquad \left[A_2(\theta)\right] = \begin{bmatrix} A_{44}(\theta) \\ A_{45}(\theta) \end{bmatrix} \tag{27}
$$

$$
\left[D_1(\theta)\right] = \begin{bmatrix} D_{12}(\theta) & D_{16}(\theta) \\ D_{22}(\theta) & D_{26}(\theta) \\ D_{26}(\theta) & D_{66}(\theta) \end{bmatrix} \qquad \left[D_2(\theta)\right] = \begin{bmatrix} D_{22}(\theta) & D_{26}(\theta) \\ D_{26}(\theta) & D_{66}(\theta) \end{bmatrix} \tag{28}
$$

Additionally, referring to the transversal load condition, the known terms in the solving equations (24) can be deduced from the external virtual work in (11):

$$
F_i = \int_{-\pi}^{\pi} \left(b \; Q_b \; \varphi_i(b,\theta) - a \; Q_a \; \varphi_i(a,\theta) \right) d\theta \; + \int_b^a \int_{-\pi}^{\pi} q(r,\theta) \; \varphi_i(r,\theta) \; d\theta \; rdr \tag{29}
$$

Aiming to the development of an innovative finite element modeling technique for composite bolted joints, the transversal load condition relevant for the definition of the novel finite element stiffness matrix consists in a force P acting on the internal rigid core alongside the z-axis of the cylindrical coordinate system, i.e. on the symmetry axis of the composite annular plate. Nevertheless, it should be noted that the rigid core is not part of the integration domain Ω defined by the annular plate, consequently the external load P is replaced by a statically equivalent distributed force per unit-length applied at the internal radius b of the annular plate $Q_b = \frac{P}{2\pi b}$.

4. Results

This Section concerns the application of the proposed analytical method to some case studies reproducing the theoretical reference model of spot joint element to verify the proposed method reliability. As previously described, they are referred to annular plates clamped on the outer radius and featuring an internal rigid core. In the following application examples, the composite annular plates bear external transversal loads consisting in a unitary force P (see Fig. 1) applied to the plate axis, along the z-axis of the cylindrical coordinate system and with the same verse.

Results from all proposed case studies are then compared with those obtained by means of refined FE models. The FE models were made using layered shell featuring 4 nodes with 6 DOFs per node.

The case studies are analyzed exploiting of rectilinear orthotropic composite annular plates realized with highly utilized lay-ups for technical applications regarding composite bolted joints, i.e. QI and 0D lay-ups as reported in Refs. [1–5, 7]. In particular, the employed stacking sequences (Table 1) and the unidirectional fiber-reinforced layer stiffness properties (Table 2) are reported in Ref. [1]; the layer thickness is $t_{lay} = 0.13$ mm.

Table 1: Lay-ups used in the numerical examples [1].

Quasi-isotropic	Zero-dominated
$[45/0/-45/90]_{5s}$	$[(45/0_2/-45/90)_3/45/0_2/-45/0]_s$

Table 2: Unidirectional fiber-reinforced layer stiffness properties [1].

E_{11} [GPa]	E_{22} [GPa]	E_{33} [GPa]	G_{12} [GPa]	G_{13} [GPa]	G_{23} [GPa]	ν_{12} [−]	ν_{13} [−]	ν_{23} [−]
140	10	10	5.2	5.2	3.9	0.3	0.3	0.5

All the numerical tests were executed with a fixed value of the overall composite annular plate thickness $t = 5.2$ mm. Besides, the impact on results accuracy of composite annular plates geometrical characteristics was investigated. In particular, three different slenderness ratios between the plate thickness t and its outer radius a were examined: 0.05, 0.075 and 0.100. This study is needed to progressively emphasize the plate shear deformability and highlight how it affects the results furnished by the proposed method and that cannot be taken into account by the methods proposed in Refs. [35, 36] which are based on the CPT.

Additionally, six different plate aspect ratios $\beta = \frac{b}{a}$ obtained trough the ratio between the inner and the outer radii of the plate were analyzed: $\beta_0 = 0.05, \beta_1 = 0.1, \beta_2 = 0.2, \beta_3 = 0.3, \beta_4 = 0.4$ and $\beta_5 = 0.5$.

The comparisons between results of the proposed analytical method (named FSDT in the Figures) and those of FE analyses are presented in the diagrams in dimensionless form, showing the distribution of the displacement components along both radial and circumferential coordinates.

Moreover, for what concerns the composite annular plate configuration characterized by slenderness ratio $\frac{t}{a} = 0.05$, which represents the upper-bound value for the application of the thin-plate theory, results obtained through the analytical method founded on the classical plate theory (named CPT in the Figures) outlined in Ref. [36] are further reported in terms of mid-surface deflection and rotations about the circumferential direction; whereas analogous outcomes for the rotations about the radial direction are not reported since their percentage variation with respect to the FE solution is too considerable.

As regards results for the mid-surface deflection, numerical results in Fig. 2 are presented in terms of dimensionless deflection, for both QI and 0D lay-ups and all the considered slenderness ratios, that is the ratio between the mid-surface deflection $w(r, 0)$ and its value at the inner edge $w(\beta, 0)$ obtained with FE analyses. These diagrams show the dimensionless deflection variation along the dimensionless radius $\rho = \frac{r}{a}$, at the angular coordinate $\theta = 0$ rad. Similarly, Fig. 3 reports for both QI and 0D lay-ups, for all the considered slenderness ratios $\frac{t}{a}$, and for an aspect ratio $\beta = 0.1$, the variation of the dimensionless mid-surface deflection along the dimensionless angle $\overline{\theta} = \frac{\theta}{\pi}$. Again, dimensionless quantities are based on the mid-surface deflection at the inner edge $w(\beta, 0)$ obtained with FE analyses. Moreover, any of these diagrams outline the circumferential variation of the mid-surface deflection at five values of the dimensionless radius: ρ=(β, 0.25, 0.40, 0.60, 0.80).

Results in Figs. 2 and 3 demonstrate that the proposed analytical method is capable of describing the composite annular plate mid-surface deflection with an excellent level of fidelity for both the dependences on the radial and the angular coordinates. Further, Table 3 reports the percentage variations Δ_β, evaluated at the inner radius $\rho = \beta$, between the results of the analytical method and the FE ones for both QI and 0D lay-ups. It is evidenced that regardless the lay-up, the slenderness and the aspect ratios the percentage variations are contained within the threshold of the numerical error, stating a significant coincidence between the outcomes of the proposed analytical method and the FE ones.

Additionally, as regards the angular variation of the mid-surface deflection (Fig. 3), the curves for $\rho = 0.40$ and 0.60 feature a more notable fluctuation with the angular coordinate, meanwhile it is less evident for $\rho = \beta$, 0.25 and 0.80 because the constrains acting on the internal and external radii tend to limit its circumferential variability. It should be noted that the mid-surface deflection for $\rho = \beta$ turns out to be not dependent on the angular coordinate θ: this confirms the capability of chosen approximation functions of fulfilling the (IV) of boundary conditions (14).

Then, according to the lay-up influence, the composite annular plates featuring QI lay-up present a maximum circumferential variation of the mid-surface deflection, for a given value of ρ, of 5%; instead, the laminates with 0D lay-up are characterized by a circumferential variation of mid-surface deflection of the order of 10%. Hence, the composite annular plates with 0D lay-up more strongly depends on the angular coordinate θ.

Table 3: Mid-surface deflection percentage variation $\Delta_{\beta_i}[\%]$, evaluated at $\rho = \beta$ for various values β_i, between analytical method and FEA for both lay-ups.

QI lay-up							
	$\frac{t}{a}$	$\Delta_{\beta_0}[\%]$	$\Delta_{\beta_1}[\%]$	$\Delta_{\beta_2}[\%]$	$\Delta_{\beta_3}[\%]$	$\Delta_{\beta_4}[\%]$	$\Delta_{\beta_5}[\%]$
CPT	0.050	−8.20	−7.55	−7.71	−8.94	−11.16	−14.83
FSDT	0.050	−0.68	−0.56	−0.31	−0.33	−0.37	−0.38
	0.075	−0.79	−0.66	−0.38	−0.63	−0.77	−0.98
	0.100	−1.11	−0.88	−0.89	−0.99	−1.17	−1.44

0D lay-up							
	$\frac{t}{a}$	$\Delta_{\beta_0}[\%]$	$\Delta_{\beta_1}[\%]$	$\Delta_{\beta_2}[\%]$	$\Delta_{\beta_3}[\%]$	$\Delta_{\beta_4}[\%]$	$\Delta_{\beta_5}[\%]$
CPT	0.050	−8.45	−7.69	−7.95	−9.36	−11.4	−15.19
FSDT	0.050	−0.71	−0.58	−0.34	−0.30	−0.37	−0.51
	0.075	−0.82	−0.61	−0.58	−0.64	−0.75	−1.02
	0.100	−1.15	−0.92	−0.88	−0.97	−1.14	−1.41

Table 4: Rotation about the circumferential direction percentage variation $\Delta_{\beta_i}[\%]$, evaluated for the maximum value at $\overline{\theta} = 0.5$, for various values β_i, between analytical method and FEA for both lay-ups.

QI lay-up							
	$\frac{t}{a}$	$\Delta_{\beta_0}[\%]$	$\Delta_{\beta_1}[\%]$	$\Delta_{\beta_2}[\%]$	$\Delta_{\beta_3}[\%]$	$\Delta_{\beta_4}[\%]$	$\Delta_{\beta_5}[\%]$
CPT	0.050	0.57	−0.61	−0.26	−0.02	0.04	0.29
FSDT	0.050	−0.26	0.20	0.06	−0.28	−0.50	0.30
	0.075	−1.00	−0.45	−0.62	−0.57	−0.85	−1.13
	0.100	−1.45	−0.97	−0.75	−1.03	−1.36	−1.73

0D lay-up							
	$\frac{t}{a}$	$\Delta_{\beta_0}[\%]$	$\Delta_{\beta_1}[\%]$	$\Delta_{\beta_2}[\%]$	$\Delta_{\beta_3}[\%]$	$\Delta_{\beta_4}[\%]$	$\Delta_{\beta_5}[\%]$
CPT	0.050	0.11	0.06	−0.45	−0.62	1.21	2.33
FSDT	0.050	−0.13	0.21	0.26	−0.43	−0.04	0.39
	0.075	−0.83	−0.23	0.17	0.38	0.49	0.56
	0.100	−1.27	−0.54	0.08	0.40	0.37	0.76

Table 5: Rotation about the radial direction percentage variation $\Delta_{\beta_i}[\%]$, evaluated for the maximum value at $\overline{\theta} = 0.5$, for various values β_i, between analytical method and FEA for both lay-ups.

QI lay-up						
$\frac{t}{a}$	$\Delta_{\beta_0}[\%]$	$\Delta_{\beta_1}[\%]$	$\Delta_{\beta_2}[\%]$	$\Delta_{\beta_3}[\%]$	$\Delta_{\beta_4}[\%]$	$\Delta_{\beta_5}[\%]$
0.050	1.92	0.77	1.13	2.44	−3.30	−11.67
0.075	3.08	1.59	−1.77	−3.07	−10.35	−14.37
0.100	2.11	0.19	−3.39	−8.01	−12.67	−15.34

0D lay-up						
$\frac{t}{a}$	$\Delta_{\beta_0}[\%]$	$\Delta_{\beta_1}[\%]$	$\Delta_{\beta_2}[\%]$	$\Delta_{\beta_3}[\%]$	$\Delta_{\beta_4}[\%]$	$\Delta_{\beta_5}[\%]$
0.050	2.52	5.78	0.90	−10.50	−11.02	−17.23
0.075	0.20	1.52	2.91	−12.86	−12.09	−16.54
0.100	−1.26	−1.66	−1.04	−11.84	−13.84	−16.86

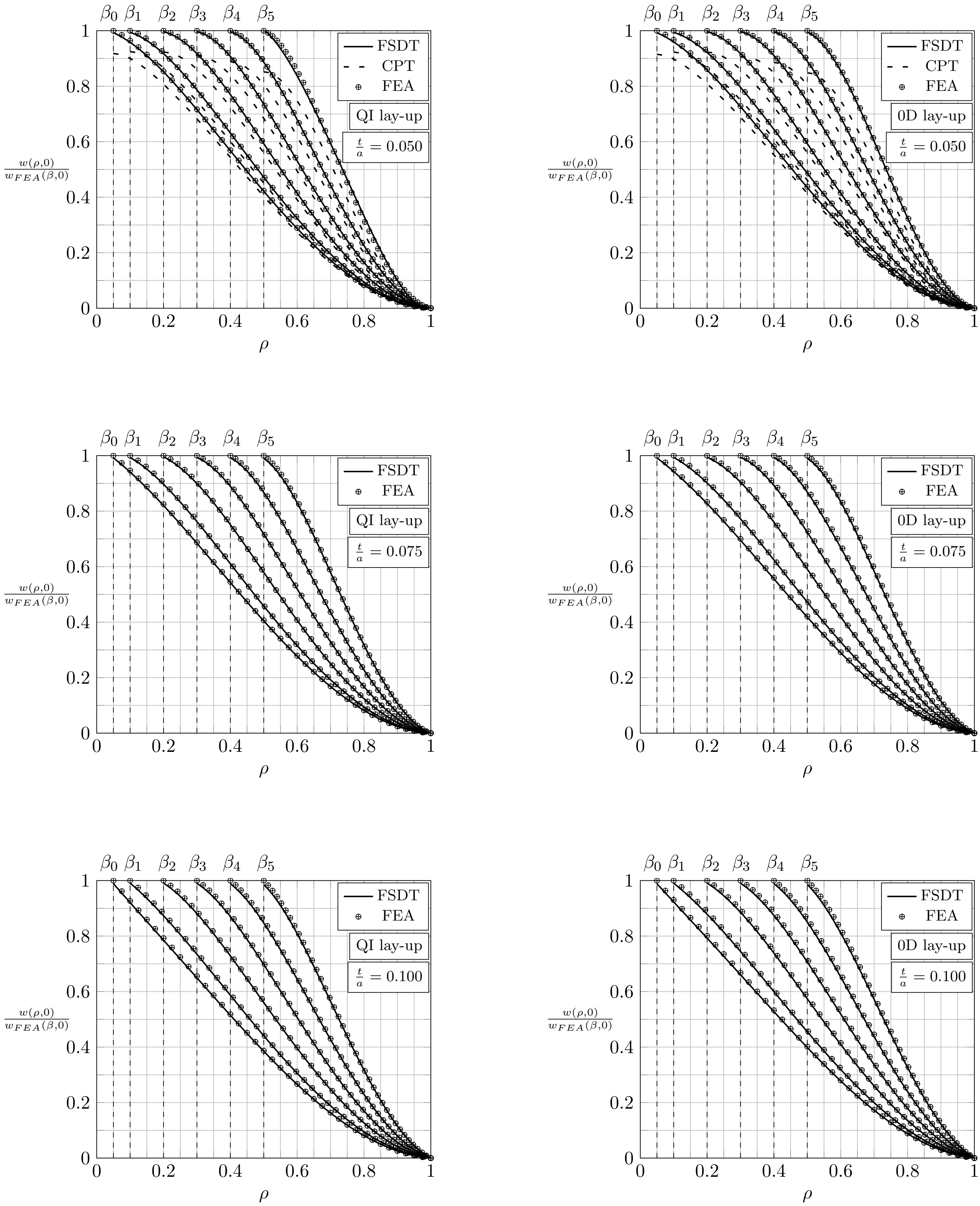

Figure 2: Curves of dimensionless mid-surface deflection as function of ρ, evaluated at $\theta = 0$ rad for different ratios $\frac{t}{a}$ and for $\beta_0 = 0.05, \beta_1 = 0.1, \beta_2 = 0.2, \beta_3 = 0.3, \beta_4 = 0.4$ and $\beta_5 = 0.5$ with QI and 0D lay-ups.

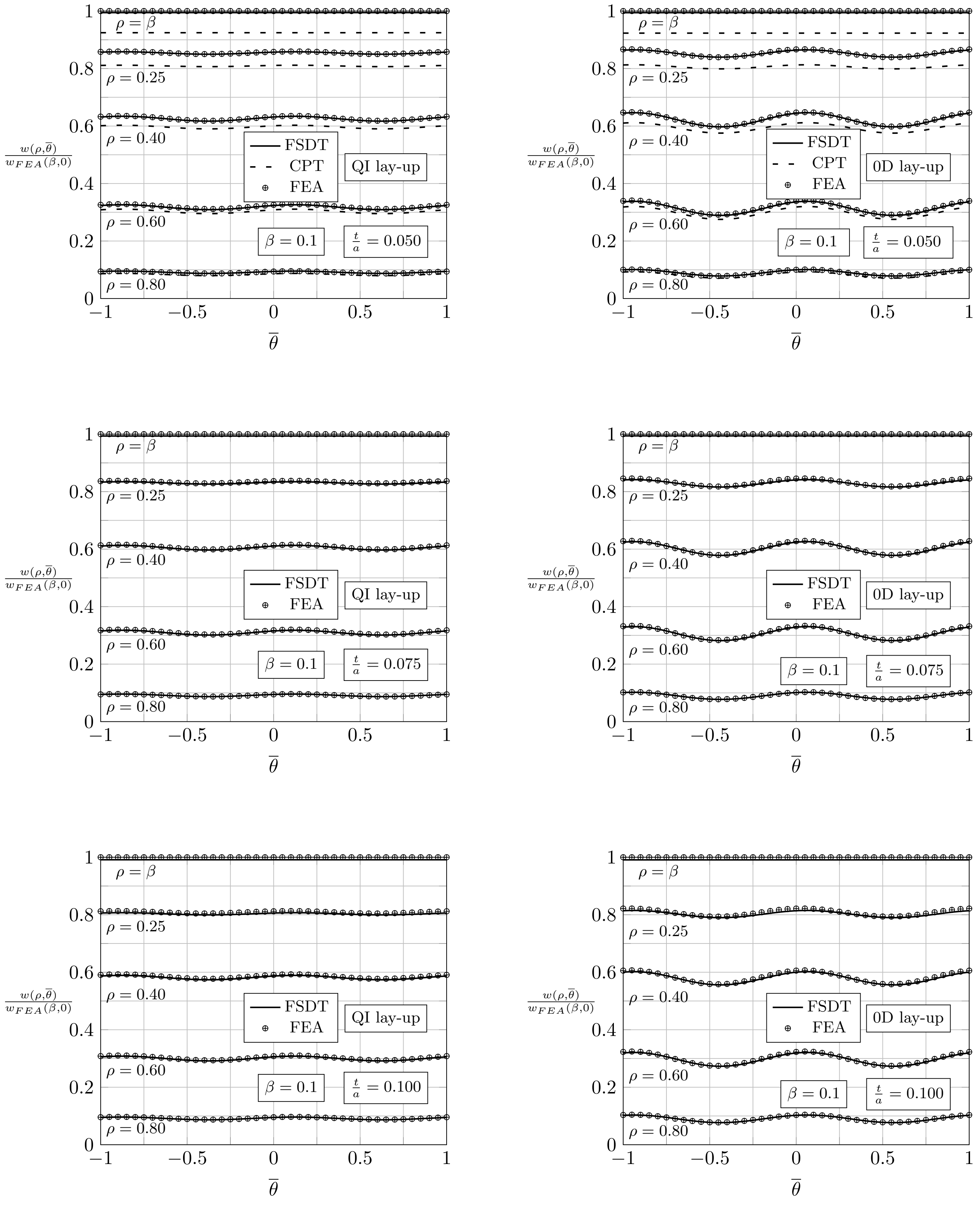

Figure 3: Curves of dimensionless mid-surface deflection as function of $\overline{\theta}$ for different ratios $\frac{t}{a}$ and $\beta = 0.1$, at ρ =(β, 0.25, 0.40, 0.60, 0.80) with QI and 0D lay-ups.

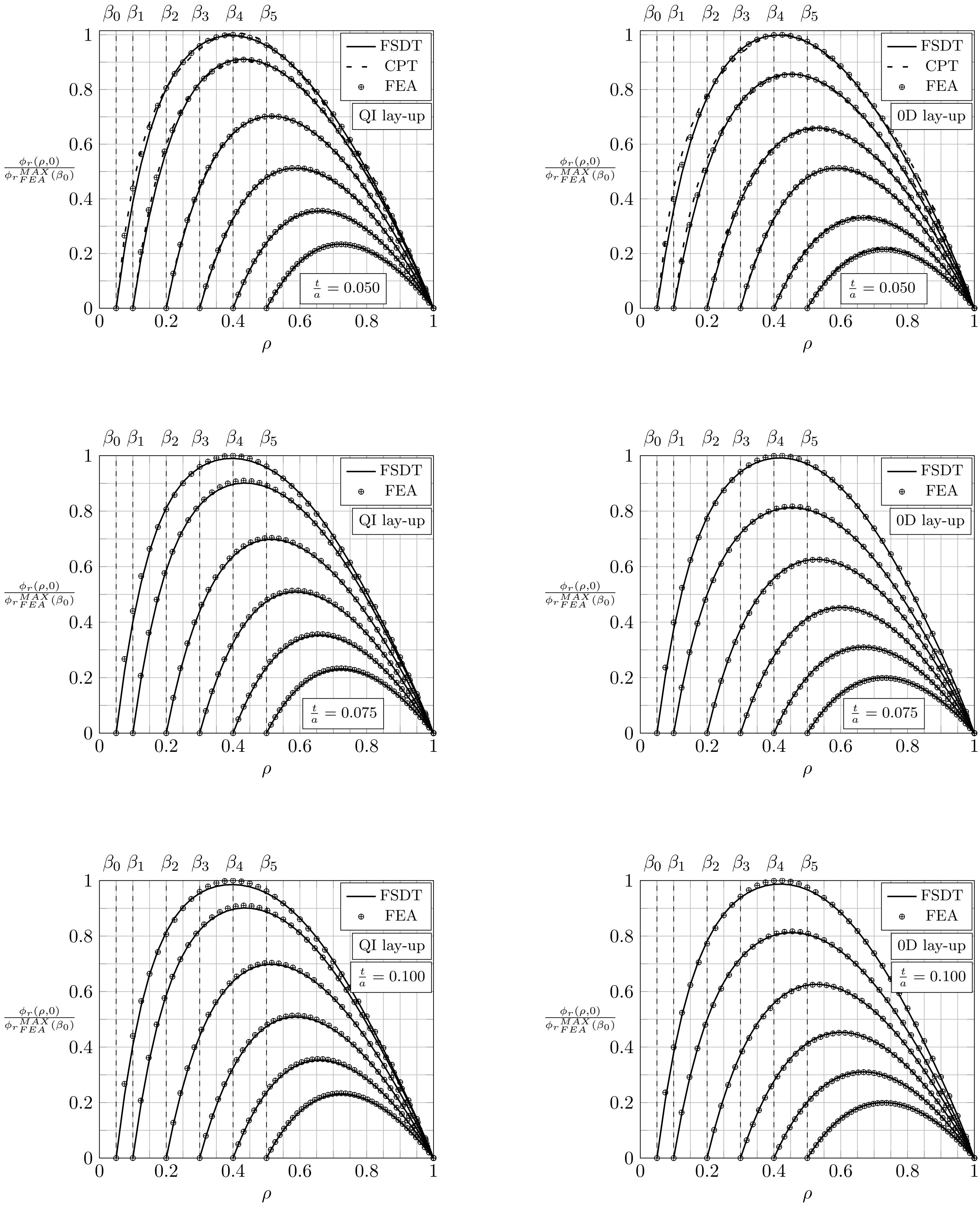

Figure 4: Curves of dimensionless rotation about the circumferential direction as function of ρ, evaluated at $\theta = 0$ rad for different ratios $\frac{t}{a}$ and for $\beta_0 = 0.05$, $\beta_1 = 0.1, \beta_2 = 0.2, \beta_3 = 0.3, \beta_4 = 0.4$ and $\beta_5 = 0.5$ with QI and 0D lay-ups.

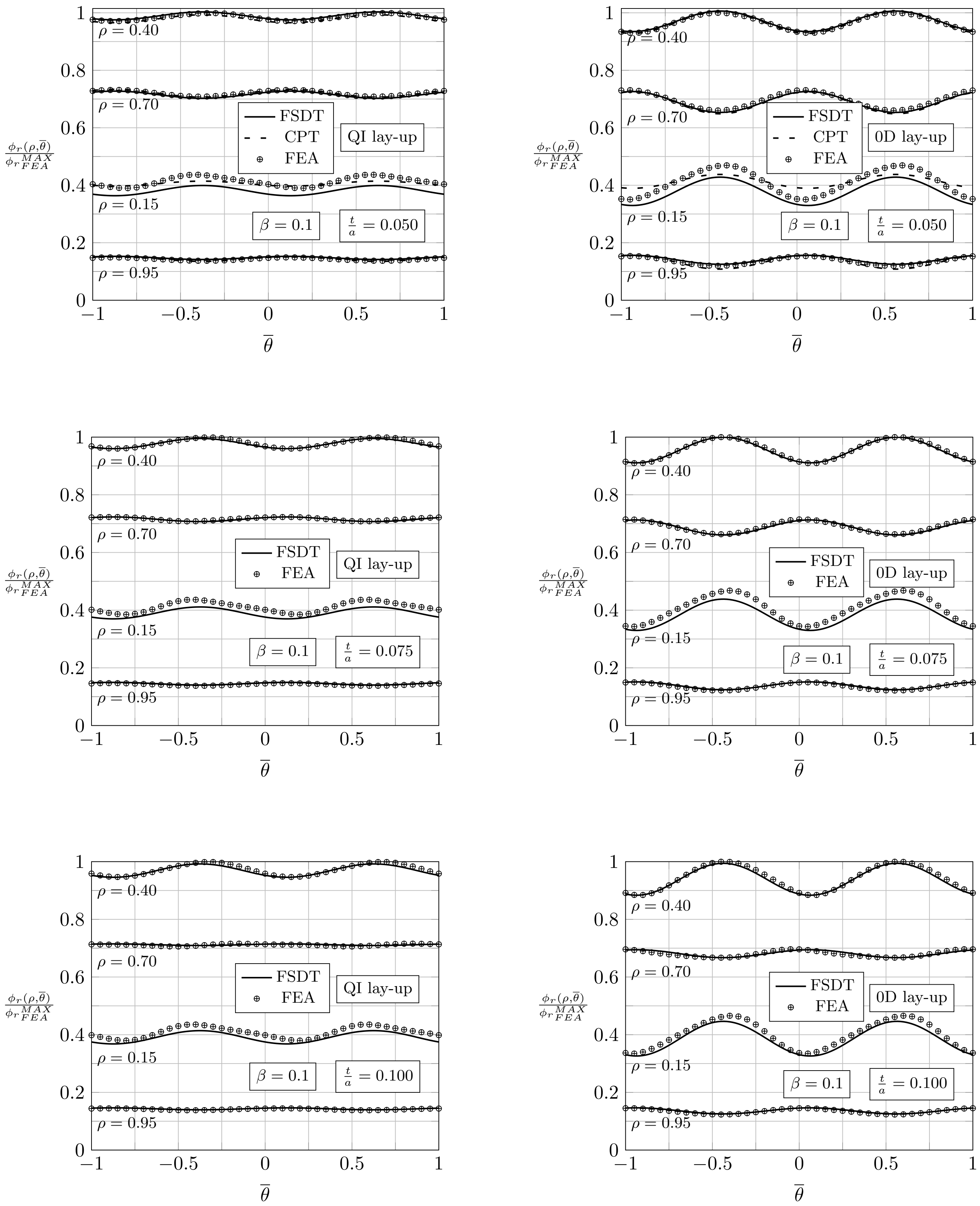

Figure 5: Curves of dimensionless rotation about the circumferential direction as function of $\overline{\theta}$ for different ratios $\frac{t}{a}$ and $\beta = 0.1$, at ρ =(β, 0.25, 0.40, 0.60, 0.80) with QI and 0D lay-ups.

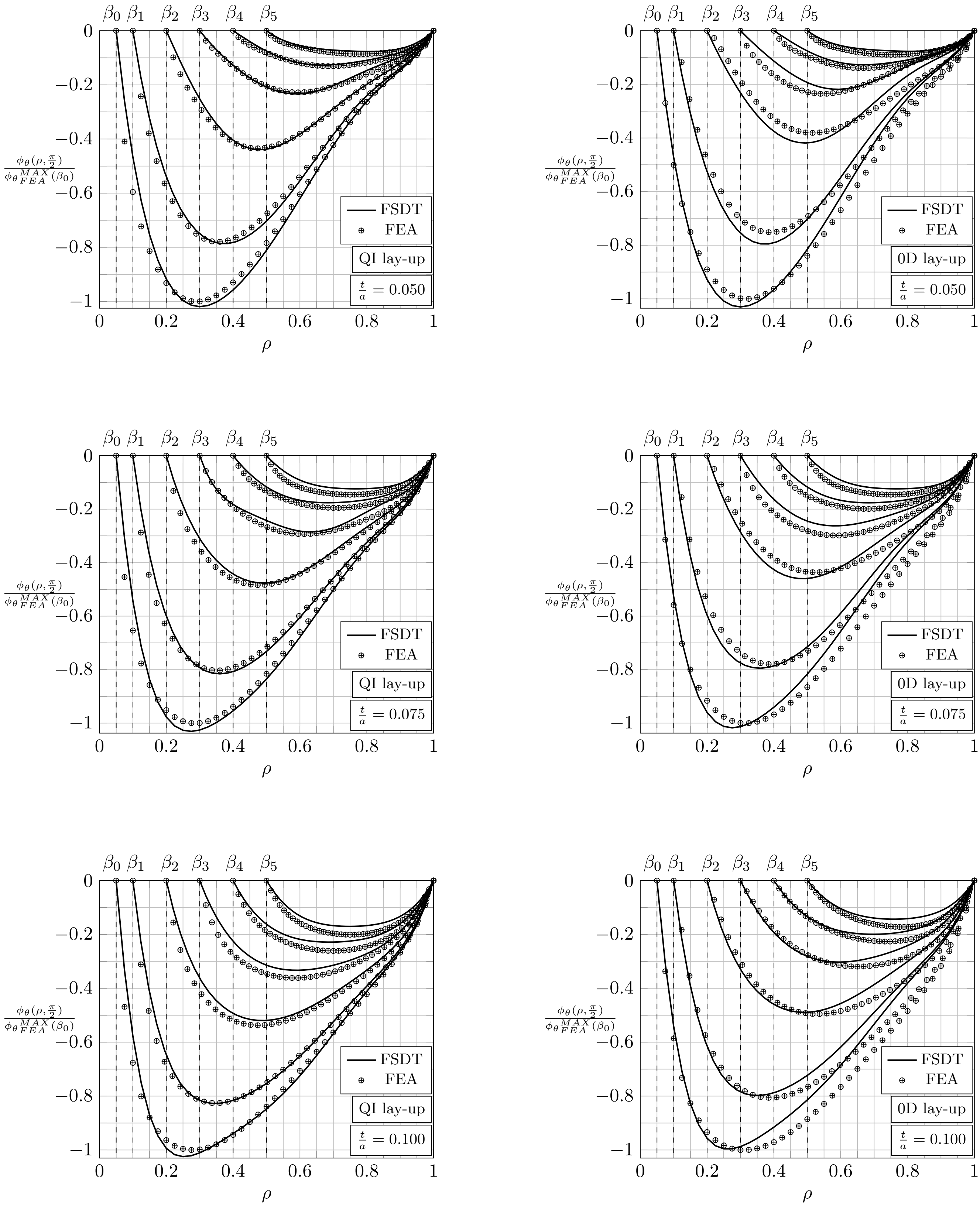

Figure 6: Curves of dimensionless rotation about the radial direction as function of ρ, evaluated at $\theta = 0$ rad for different ratios $\frac{t}{a}$ and for $\beta_0 = 0.05, \beta_1 = 0.1, \beta_2 = 0.2, \beta_3 = 0.3, \beta_4 = 0.4$ and $\beta_5 = 0.5$ with QI and 0D lay-ups.

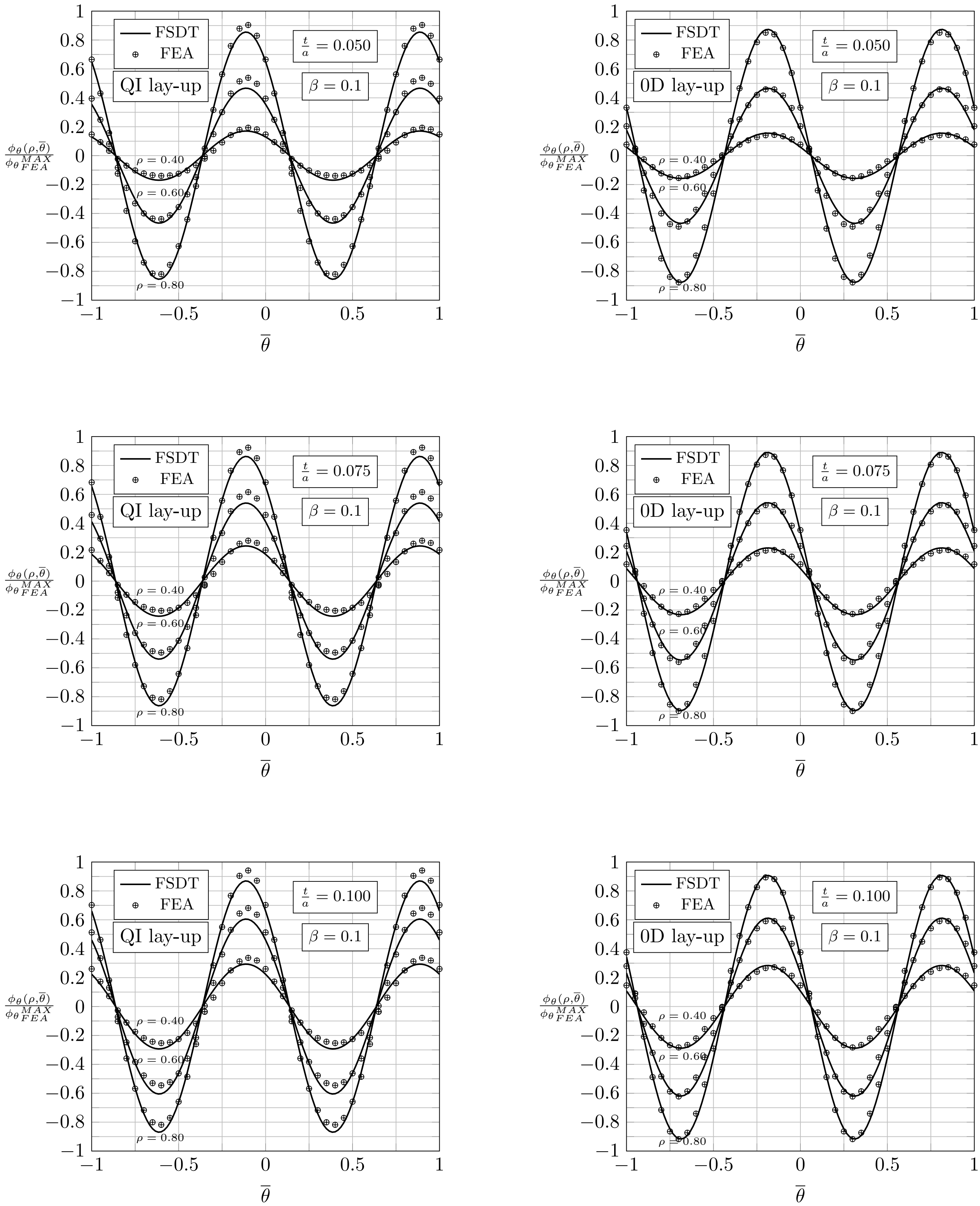

Figure 7: Curves of dimensionless rotation about the radial direction as function of $\overline{\theta}$ for different ratios $\frac{t}{a}$ and β = 0.1, at ρ =(β, 0.25, 0.40, 0.60, 0.80) with QI and 0D lay-ups.

Furthermore, the comparison between the methods based on the FSDT and on the CPT for the plate configuration with slenderness ratio $\frac{t}{a}$ = 0.05 reveals that the percentage variations Δ_β observed in the results derived by means of the analytical method described in Ref. [36] can be abated, for all the considered aspect ratios, taking into account the plate shear deformability, i.e. exploiting the proposed analytical method. Thus, the slenderness ratio $\frac{t}{a}$ = 0.05 can be considered as an indicative threshold value between the application field of the thin-plate theory and the range where the contribution of the plate shear deformability cannot be neglected.

Besides, Figs. 4 and 6 summarize, for both lay-ups, results regarding the variation along the dimensionless radial coordinate ρ of the dimensionless forms of the rotations about the circumferential and the radial coordinates, respectively, that are obtained through the ratios between the functions $\phi_r(\rho, 0)$ and $\phi_\theta(\rho, \frac{\pi}{2})$ and their maximum values obtained by means of FE analyses with aspect ratio β_0. In addition, the circumferential variation of the rotation components is shown in dimensionless form in Figs. 5 and 7, for the shape factor $\beta = 0.1$, against the dimensionless angular coordinate $\overline{\theta}$; dimensionless quantities are based on the maximum value of rotation components obtained with FE analyses. Different specific values of the dimensionless radii are considered: ρ=(β, 0.20, 0.40, 0.60 and 0.80) for the rotation about the circumferential direction and ρ=(0.40, 0.60 and 0.80) for the rotation about the radial direction.

As for the mid-surface deflection, both the radial and the circumferential variations of the rotation ϕ_r (Figs. 4 and 5) are described with high precision by the proposed analytical method. Observing the curves for this rotation component against the dimensionless radial coordinate ρ (Fig. 4), it should be noticed that, for every aspect ratio β_i and both lay-ups, the maximum value of the functions ϕ_r is located at a radial coordinate which is approximately distant 0.3 from the inner edge of the composite annular plate.

Moreover, the neglect of the plate shear deformation does not significantly affect the results accuracy as demonstrated by the results obtained making use of the CPT. Table 4 outlines the percentage variation Δ_β in correspondence of the radial coordinate where the maximum rotation is measured by the FE analyses. Even in this case the percentage variation is attributable to the numerical approximation and, subsequently, the agreement between the results of the proposed analytical method and those obtained by FE analyses is highly confirmed.

Once again the lay-up has direct influence on the variation of the displacement component with the angular coordinate. Indeed, as reported in Fig. 5, the composite annular plates characterized by 0D lay-up show a more evident angular variation of the rotation about the circumferential direction with respect to the plates featuring the QI lay-up. Nevertheless, the influence of the constraints present at the inner and at the outer edges of the annular plate on this displacement component is different from the one experienced by the mid-surface deflection. In this regard, the curves with ρ = 0.15 and 0.40 show a more pronounced dependence on the angular coordinate whereas the effect is more mitigated if the rotation about the circumferential direction is evaluated at ρ = 0.70 and 0.90; it can be deduced that the rotation about the circumferential direction is more angularly variable in the plate portion enclosed by the inner radius and the radial coordinate where ϕ_r assumes its maximum value.

According to the rotation about the radial direction, the deviation between the solution of the proposed analytical method and the FE one is more considerable in comparison with those of the other displacement components, even though it is still very acceptable.

In reference to Table 5, it can be concluded that the outcomes turn out to be not particularly influenced by the slenderness ratio of the plate, meanwhile the effect of the aspect ratio is more remarkable for both QI and 0D lay-ups. In fact, the percentage variations Δ_β are limited for the aspect ratios β_0 - β_2, whereas they undergo an increase when higher values of the aspect ratio are taken into account.

Overall, as regards the variation along the radius (Fig. 6), results for composite annular plates featuring QI lay-up better agree with FE reference solution. In addition, Fig. 7, the analytical method appropriately match the circumferential variability of the rotation about the radial direction.

5. Conclusions

A novel solution approach based on Ritz method and in the framework of the first-order shear deformation theory for rectilinear orthotropic composite annular plate undergoing transversal loads was outlined.

The analytical study of the transversal load condition is a needed in order to accomplish the theoretical definition of an innovative finite element with the capability of accurately modeling composite bolted joints along with a modest quantitative of DOFs, exploiting the Spot Element simulation technique described in Ref. [13]. This solution is needed to evaluate the corresponding terms of the Spot Element stiffness matrix. For that purpose, the theoretical reference model of composite bolted joints was employed an externally clamped rectilinear orthotropic composite annular plate featuring an internal rigid core. In this regard, a new analytical methodology for the bending analysis of rectilinear orthotropic composite circular plates undergoing orthogonal loads was defined accounting for shear deformability.

Solutions were provided making use of Ritz method, so, at first, the rectilinear orthotropic composite circular plates were characterized in the framework of the first-order shear deformation theory: the stress resultants, in-plane forces and bending and torque moments, were derived in cylindrical coordinates.

Then, the general expression of the principle of virtual works was outlined and specified for the external load condition. The unknown displacement components were written in discretized form through the formulations of original approximation functions compliant with both essential and natural boundary conditions of the problem. The approximated form of the mid-surface deflection and of the rotations about the circumferential and the radial directions were split into a contribution not-dependent on the angular coordinate θ and into a contribution needed to account for their circumferential variation, due to the not-axisymmetry of the material properties.

The generalized form of the system of linear equations for the transversal load condition is reported and solved for some case studies. In order to assess the effect of the plate shear deformability on results accuracy, the influence of the slenderness ratio variation on the results was investigated; demonstrating that the proposed analytical method is capable of accurately taking into account this effect. Furthermore, the effect of the plate aspect ratio was also analyzed.

Results of the original proposed method were compared to those obtained by means of FEA performed with a refined reference model, obtaining a good agreement. A quasi-isotropic and a zero-dominated stacking sequences symmetrical in reference to the plate mid-surface are employed for the case studies because of their widespread employment in the realization of composite materials components to be connected with bolted joints.

The results of the original proposed method were exhibited along with the FE analyses ones, considering a refined reference model, demonstrating a very good agreement.

Appendix A

As described in Section 3, the numerical examples were realized making use of series $W_N(r,\theta)$, $\Phi_r^N(r,\theta)$ and $\Phi_\theta^N(r,\theta)$ composed of 10 terms; in particular, 5 terms series to represent the medium and axisymmetric contribution of displacement component and 5 for the not-axisymmetric ones. The approximation functions $\varphi_j(r)$ and the functions $p(r)$ employed in the numerical examples are of polynomial type revealed to possess no general and repetitive expression.

Consequently, the polynomial functions $\varphi_j(r)$ employed for the realization of the case studies, which encompass polynomials from the first to the fifth degree, are hereafter reported:

$$\varphi_1(r) = r - a$$

$$\varphi_2(r) = \Big(r - a\Big)\Big(r + a + 1\Big)$$

$$\varphi_3(r) = \Big(r - a\Big)\Big(r^2 + (a + 1)r + a^2 + a + 1\Big)$$

$$\varphi_4(r) = \Big(r - a\Big)\Big(r^3 + (a + 1)r^2 + (a^2 + a + 1)r + a^3 + a^2 + a + 1\Big)$$

$$\varphi_5(r) = \Big(r - a\Big)\Big(r^4 + (a + 1)r^3 + (a^2 + a + 1)r^2 + (a^3 + a^2 + a + 1)r + a^4 + a^3 + a^2 + a + 1\Big)$$

Appendix B

Furthermore, the polynomial functions from $p_1(r)$ to $p_5(r)$, ranging from a first degree polynomial function in the variable r until a sixth degree one, are:

$$p_1(r) = \Big(r - a\Big)\Big(r - b\Big)$$

$$p_2(r) = \Big(r - a\Big)\Big(r - b\Big)\Big(r + a + b + 1\Big)$$

$$p_3(r) = \Big(r - a\Big)\Big(r - b\Big)\Big(r^2 + (a + b + 1)r + a^2 + ab + b^2 + a + b + 1\Big)$$

$$p_4(r) = \Big(r - a\Big)\Big(r - b\Big)\Big(r^3 + (a + b + 1)r^2 + (a^2 + ab + b^2 + a + b + 1)r + a^3 + a^2b + ab^2 + b^3 + a^2 + ab + b^2 + a + b + 1\Big)$$

$$p_5(r) = \Big(r - a\Big)\Big(r - b\Big)\Big(r^4 + (a + b + 1)r^3 + (a^2 + ab + b^2 + a + b + 1)r^2 + (a^3 + a^2b + ab^2 + b^3 + a^2 + ab + b^2 + a + b + 1)r + \\ + a^4 + a^3b + a^2b^2 + ab^3 + b^4 + a^3 + a^2b + ab^2 + b^3 + a^2 + ab + b^2 + a + b + 1\Big)$$

$$p_6(r) = \Big(r - a\Big)\Big(r - b\Big)\Big(r^4 + (a + b + 1)r^3 + (a^2 + ab + b^2 + a + b + 1)r^2 + (a^3 + a^2b + ab^2 + b^3 + a^2 + ab + b^2 + a + b + 1)r + \\ + a^4 + a^3b + a^2b^2 + ab^3 + b^4 + a^3 + a^2b + ab^2 + b^3 + a^2 + ab + b^2 + a + b + 1\Big)$$

References

[1] M. A. McCarthy, C. T. McCarthy, V. P. Lawlor, W. F. Stanley, Three-dimensional finite element analysis of single-bolt, single-lap composite bolted joints: part I - model development and validation, Composite Structures 71 (2005) 140–158.

[2] C. T. McCarthy, M. A. McCarthy, Three-dimensional finite element analysis of single-bolt, single-lap composite bolted joints: Part II effects of bolt-hole clearance, Composite Structures 71 (2005) 159–175.

[3] P. J. Gray, C. T. McCarthy, A global bolted joint model for finite element analysis of load distributions in multi-bolt composite joints, Composites Part B: Engineering 41 (2010) 317–325.

[4] P. J. Gray, C. T. Mccarthy, A highly efficient user-defined finite element for load distribution analysis of large-scale bolted composite structures, Composites Science and Technology 71 (2011) 1517–1527.

[5] Z. Kapidžić, L. Nilsson, H. Ansell, Finite element modeling of mechanically fastened composite-aluminum joints in aircraft structures, Composite Structures 109 (2014) 198–210.

[6] N. M. Chowdhury, W. K. Chiu, J. Wang, P. Chang, Experimental and finite element studies of bolted, bonded and hybrid step lap joints of thick carbon fibre/epoxy panels used in aircraft structures, Composites Part B: Engineering 100 (2016) 68–77.

[7] Y. Zhou, H. Yazdani Nezhad, C. Hou, X. Wan, C. T. McCarthy, M. A. McCarthy, A three dimensional implicit finite element damage model and its application to single-lap multi-bolt composite joints with variable clearance, Composite Structures 131 (2015) 1060–1072.

[8] P. Liu, X. Cheng, S. Wang, S. Liu, Y. Cheng, Numerical analysis of bearing failure in countersunk composite joints using 3D explicit simulation method, Composite Structures 138 (2016) 30–39.

[9] Q. Zhang, X. Cheng, J. Zhang, S. Wang, Y. Cheng, T. Zhang, Experimental and numerical investigation of composite box joint under tensile load, Composites Part B: Engineering 107 (2016) 75–83.

[10] X. Cheng, S. Wang, J. Zhang, W. Huang, Y. Cheng, J. Zhang, Effect of damage on failure mode of multi-bolt composite joints using failure envelope method, Composite Structures 160 (2017) 8–15.

[11] V. G. Belardi, P. Fanelli, F. Vivio, Structural analysis and optimization of anisogrid composite lattice cylindrical shells, Composites Part B: Engineering 139 (2018) 203–215.

[12] V. G. Belardi, P. Fanelli, F. Vivio, Design, analysis and optimization of anisogrid composite lattice conical shells, Composites Part B: Engineering 150 (2018) 184–195.

[13] F. Vivio, A new theoretical approach for structural modelling of riveted and spot welded multi-spot structures, International Journal of Solids and Structures 46 (2009) 4006–4024.

[14] F. Di Cicco, P. Fanelli, F. Vivio, Fatigue reliability evaluation of riveted lap joints using a new rivet element and DFR, International Journal of Fatigue 101 (2017) 430–438.

[15] P. Fanelli, F. Vivio, A general formulation of an analytical model for the elastic-plastic behaviour of a spot weld finite element, Mechanics Research Communications 69 (2015) 54–65.

[16] S. G. Lekhnitskii, S. W. Tsai, T. Cheron, Anisotropic Plates, Translated from the second Russian edition by S.W. Tsai and T. Cheron, Gordon and Breach, Gordon and Breach, Science Publishers, Inc., New York, 1968.

[17] S. Timoshenko, S. Woinowsky-Krieger, Theory of plates and shells, McGraw-Hill, New York, 2nd edition, 1959.

[18] S. Tang, Stability of a laminated anisotropic circular plate, Journal of Spacecraft and Rockets 9 (1972) 123–124.

[19] C. Chang-Jun, D. Wei, D. F. Parker, Elastic instability of polar orthotropic annular plates, International Journal of Engineering Science 27 (1989) 109–121.

[20] L. Fu, A. M. Waas, Buckling of polar and rectilinearly orthotropic annuli under uniform internal or external pressure loading, Composite Structures 22 (1992) 47–57.

[21] R. Seifi, N. Khoda-yari, H. Hosseini, Study of critical buckling loads and modes of cross-ply laminated annular plates, Composites Part B: Engineering 43 (2012) 422–430.

[22] N. R. Rajappa, Free vibration of rectangular and circular orthotropic plates, AIAA Journal (1963) 1194–1195.

[23] S. B. Dong, A. E. Lopez, Natural vibrations of a clamped circular plate with rectilinear orthotropy by least-squares collocation, International Journal of Solids and Structures 21 (1985) 515–526.

[24] L. G. Nallim, R. O. Grossi, Natural frequencies of symmetrically laminated elliptical and circular plates, International Journal of Mechanical Sciences 50 (2008) 1153–1167.

[25] S. Hosseini-Hashemi, M. Azimzadeh-Monfared, H. Rokni Damavandi Taher, A 3-D Ritz solution for free vibration of circular/annular functionally graded plates integrated with piezoelectric layers, International Journal of Engineering Science 48 (2010) 1971–1984.

[26] M. Salehi, A. R. Sobhani, Elastic linear and non-linear analysis of fiber-reinforced symmetrically laminated sector Mindlin plate, Composite Structures 65 (2004) 65–79.

[27] A. Andakhshideh, S. Maleki, M. M. Aghdam, Non-linear bending analysis of laminated sector plates using generalized differential quadrature, Composite Structures 92 (2010) 2258–2264.

[28] M. Kadkhodayan, A. Erfani Moghadam, G. J. Turvey, J. Alamatian, A DXDR large deflection analysis of uniformly loaded square, circular and elliptical orthotropic plates using non-uniform rectangular finite-differences, Journal of Mechanical Science and Technology 26 (2012) 3231–3242.

[29] M. E. Golmakani, M. Kadkhodayan, Large deflection thermoelastic analysis of functionally graded stiffened annular sector plates, International Journal of Mechanical Sciences 69 (2013) 94–106.

[30] M. E. Golmakani, Nonlinear bending analysis of ring-stiffened functionally graded circular plates under mechanical and thermal loadings, International Journal of Mechanical Sciences 79 (2014) 130–142.

[31] M. Jabbari, E. Shahryari, H. Haghighat, M. R. Eslami, An analytical solution for steady state three dimensional thermoelasticity of functionally graded circular plates due to axisymmetric loads, European Journal of Mechanics - A/Solids 47 (2014) 124–142.

[32] S. Maleki, M. Tahani, Bending analysis of laminated sector plates with polar and rectilinear orthotropy, European Journal of Mechanics - A/Solids 40 (2013) 84–96.

[33] N. P. Patel, D. S. Sharma, Bending of composite plate weakened by square hole, International Journal of Mechanical Sciences 94-95 (2015) 131–139.

[34] V. G. Belardi, P. Fanelli, F. Vivio, Structural analysis of transversally loaded quasi-isotropic rectilinear orthotropic composite circular plates with Galerkin method, Procedia Structural Integrity 8 (2018) 368–378.

[35] V. G. Belardi, P. Fanelli, F. Vivio, Bending analysis with Galerkin method of rectilinear orthotropic composite circular plates subject to transversal load, Composites Part B: Engineering 140 (2018) 250–259.

[36] V. G. Belardi, P. Fanelli, F. Vivio, Elastic analysis of rectilinear orthotropic composite circular plates subject to transversal and in-plane load conditions using Ritz method, Composite Structures 199 (2018) 63–75.

[37] V. G. Belardi, P. Fanelli, F. Vivio, Ritz method analysis of rectilinear orthotropic composite circular plates undergoing in-plane bending and torsional moments, Mechanics of Advanced Materials and Structures (2019) Under Review.

[38] V. G. Belardi, P. Fanelli, F. Vivio, A novel composite bolted joint element: application to a single-bolted joint, Procedia Structural Integrity 12 (2018) 281–295.

[39] R. M. Jones, Mechanics of composite materials, Scripta Book Company Washington DC, 1975.

[40] C. M. Wang, J. N. Reddy, K. H. Lee, Shear deformable beams and plates: relationships with classical solutions, Elsevier, 2000.
[41] J. N. Reddy, Theory and analysis of elastic plates and shells, CRC press, 2006.